A compact wideband dielectric resonator antenna with optimized inhomogeneous material distribution

Trupti Bellundagi✉ and Binbin Yang
Electrical and Computer Engineering, North Carolina A&T State University, Greensboro, North Carolina, USA
✉E-mail: tbellundagi@aggies.ncat.edu

This article proposes a novel compact wideband dielectric resonator antenna design that incorporates inhomogeneous material distribution in a cubic structure. Specifically, in this design, the cubic dielectric resonator antenna is divided into multiple small blocks, and a continuous genetic algorithm is employed to optimize the material property of each block in order to maximize the radiation bandwidth. As a result, a cubic dielectric resonator antenna with inhomogeneous material distributions is designed and tested. In measurement, the proposed compact dielectric resonator antenna design exhibits 64.9% impedance bandwidth (4.08–8 GHz), considerably higher than the bandwidth of the initial homogeneous dielectric resonator antenna. The maximum system gain achieved over the frequency range is 9 dB at 7 GHz, with a peak measured system efficiency of 90.6%.

Introduction: Dielectric resonator antennas (DRA) leverage a dielectric resonator body as the main radiator [1]. In contrast with metallic antennas, which suffer from conductive losses, a DRA boasts superior radiation efficiency at high microwave and mm-wave frequencies [2–4] and can be designed with a vast range of material options and 3-dimensional (3D) geometries [5]. Due to their compact size, low loss characteristics, and ease of integration with other electronic components, DRAs have gained significant attention in recent years and found applications in modern wireless communication systems, radar systems, mobile networks, and satellite communications [6–8].

The performance of a DRA is fundamentally dependent on its 3D geometry and the material properties, including its permittivity and loss tangent [5]. In earlier years, wideband DRA designs have focused largely on customizing the shape of the DRAs to realize new radiation characteristics [9–12]. However, it is worth noting that by carefully selecting and distributing materials within the dielectric body, it is also possible to tailor the antenna's radiation characteristics, as manifested by the wideband DRA designs through stacked/step-index structures [13–15]. Specifically, the material distribution within the dielectric body of a DRA could considerably impact its bandwidth by tailoring the electromagnetic field distribution and resonant modes [16]. The variation of material also allows for better impedance matching over a broader frequency range, reducing reflection losses [17]. The optimization of the material distribution within the DRA can also enhance the antenna's ability to excite higher order modes, which further expands the operational bandwidth [18]. In summary, material distribution optimization is a powerful approach to meet the demanding bandwidth requirements of modern wideband wireless communication systems. The continuing innovations in novel fabrication techniques and material science also support DRA designs with complex shapes and material distributions [18–20].

To the best of the authors' knowledge, there is limited investigation on how inhomogeneous material distribution would impact a DRA's radiation characteristics and the benefits it could bring. This work intends to address this issue and provide a unique design case in the wideband DRA setting. Instead of limiting the design to stacked structures as was conventionally done, this work proposes to discretize the entire DRA volume and allow any internal portion of the DRA to possess varying material properties. Specifically, this approach utilizes a genetic algorithm (GA) to determine the optimal combination of materials within the dielectric body. By leveraging the capabilities of GA, we can efficiently explore a vast search space to identify the material configurations that result in a significantly wider bandwidth.

The GA iteratively refines the material distribution by simulating evolutionary processes such as selection, crossover, and mutation, thereby converging on the most effective design [21]. This method allows us to tailor the dielectric properties within the resonator precisely, achieving superior impedance matching and supporting multiple resonant modes. As a result, our optimized DRA design exhibited enhanced bandwidth, making it highly suitable for modern wireless communication systems that demand high performance and reliability. This article presents the detailed design methodology, simulation and measurement results, and the performance analysis of the proposed wideband DRA.

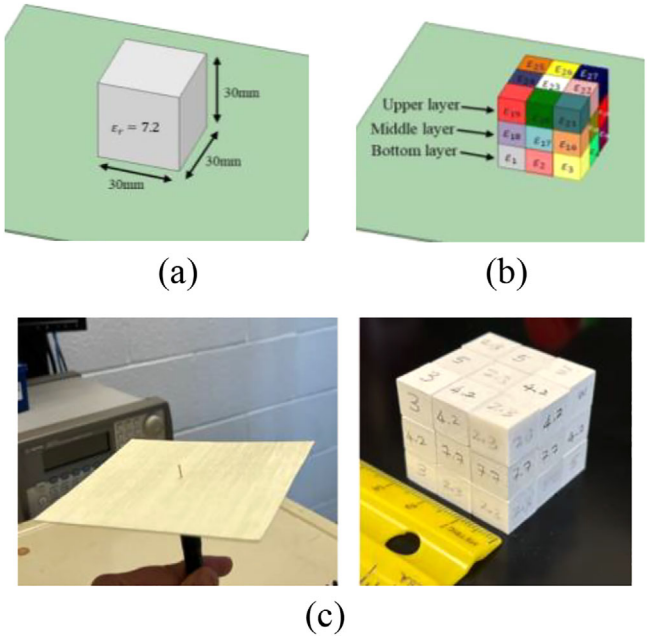

Fig. 1 *Proposed dielectric resonator antenna (DRA) with optimized inhomogeneous material distributions: (a) initial solid block DRA, (b) optimized DRA with different materials, (c) the coaxial probe type feed and DRA prototype*

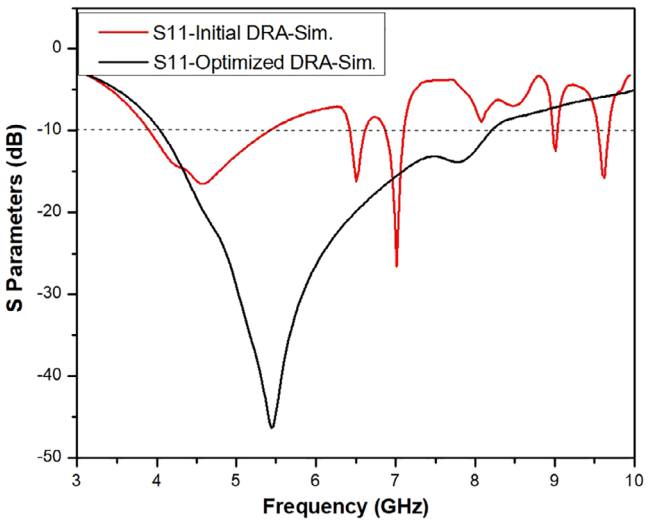

Fig. 2 *Simulated S parameters of the initial dielectric resonator antenna (DRA) (red) and optimized DRA (black)*

Design of the wideband DRA: The initial cube DRA is shown in Figure 1a, with a dimension of $w = 30$, $l = 30$, and $h = 30$ mm. The dimensions of the initial DRA can be different depending on the space available for a specific application. The dielectric constant of the initial DRA was 7.2 with a loss tangent of 0.006. It was mounted on top of a microstrip substrate (Rogers RO4350) with a thickness of 0.76 mm. A coaxial probe of 7 mm in height feeds the DRA in the centre. The *S* parameter of the initial DRA is shown in Figure 2 as the red curve, which indicates a 10 dB bandwidth of 31.7% (3.92–5.4 GHz).

In order to further widen the bandwidth of the DRA, we chose to explore the design space in the material distribution within the DRA.

Table 1. The dielectric constants of each block in the optimized dielectric resonator antenna (DRA) with the adjusted dielectric constants in parentheses

Layer	Dielectric constants		
Bottom	$\varepsilon_7 =$ 6.96 (7.7)	$\varepsilon_8 =$ 1.74 (2.3)	$\varepsilon_9 =$ 2.24 (2.3)
	$\varepsilon_6 =$ 6.49 (6.0)	$\varepsilon_5 =$ 5.15 (5.0)	$\varepsilon_4 =$ 1.60 (2.3)
	$\varepsilon_1 =$ 3.03 (3.0)	$\varepsilon_2 =$ 1.75 (2.3)	$\varepsilon_3 =$ 2.92 (3.0)
Middle	$\varepsilon_{12} =$ 7.11 (7.7)	$\varepsilon_{11} =$ 6.19 (5.0)	$\varepsilon_{10} =$ 4.16 (3.0)
	$\varepsilon_{13} =$ 4.31 (4.2)	$\varepsilon_{14} =$ 7.09 (7.7)	$\varepsilon_{15} =$ 7.04 (7.7)
	$\varepsilon_{18} =$ 3.90 (4.2)	$\varepsilon_{17} =$ 7.17 (7.7)	$\varepsilon_{16} =$ 6.96 (7.7)
Upper	$\varepsilon_{25} =$ 1.75 (2.3)	$\varepsilon_{26} =$ 5.07 (5.0)	$\varepsilon_{27} =$ 3.23 (3.0)
	$\varepsilon_{24} =$ 5.86 (5.0)	$\varepsilon_{23} =$ 1.53 (2.3)	$\varepsilon_{22} =$ 3.98 (4.2)
	$\varepsilon_{19} =$ 3.06 (3.0)	$\varepsilon_{20} =$ 4.35 (4.2)	$\varepsilon_{21} =$ 2.43 (2.3)

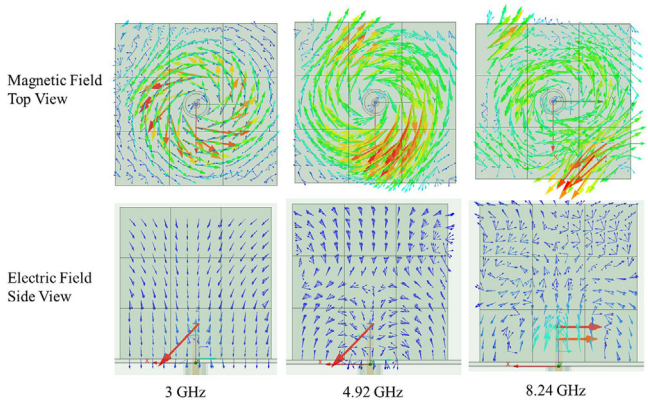

Fig. 3 *Magnetic and Electric Fields distribution of optimized dielectric resonator antenna (DRA) at 3, 4.92, and 8.24 GHz*

Specifically, the initial DRA was segmented into 3 vertical and horizontal sections, creating a total of 27 individual cubes, each with dimensions of 10 mm. These cubes are arranged in three layers (bottom, middle, and upper) each layer consisting of nine blocks, as illustrated in Figure 1b. We can choose any size for small sections according to the ease of fabrication. The smaller the size of the section, the larger design and search space we will have, and the better potential performance we can achieve. Each block was assigned with a permittivity variable within a given range. In this case, each block's permittivity varied from 1.5 to 7.2. We can change the range of material permittivity according to availability of material for fabrication. Then, the optimization was conducted using the GA in Ansys HFSS, with a population size of 50, a crossover probability of 0.5, and a mutation rate of 0.2. The GA process varies the dielectric constant of each block evolutionarily and searches for the optimal combination of dielectric constants that results in $S_{11} < -10$ dB within the frequency range of interest (4–8.5 GHz). Figure 1b shows the optimized DRA, where different colours were assigned to each block to indicate different material dielectric constants. The optimized dielectric constants for the lowest cost case scenario are listed in Table 1. In real implementation, the dielectric constants will be rounded to the nearest material properties available from the manufacturer. The *S* parameter of the optimized DRA is shown in Figure 2 in the black curve. We can see the improvement in bandwidth compared to the initial DRA. The optimized DRA achieves bandwidth of 68.8% (4.04–8.28 GHz) in contrast with the initial DRA's bandwidth of 31.7% (3.92–5.4 GHz).

The structure is excited in the centre using a probe, the basic mode excited is equivalent to the TM^z_{111} mode in a rectangular DRA [22, 23], and higher order TM modes will be excited at higher frequencies. To better illustrate this, three antenna resonances (zero reactance) are identified from the Z parameter as 3, 4.92, and 8.24 GHz. The magnetic and electric field distributions within the DRA at the three resonance frequencies are provided in Figure 3. The fields at 3 GHz obviously resemble that of the TM^z_{111} mode, and higher TM^z mode field distributions are observed

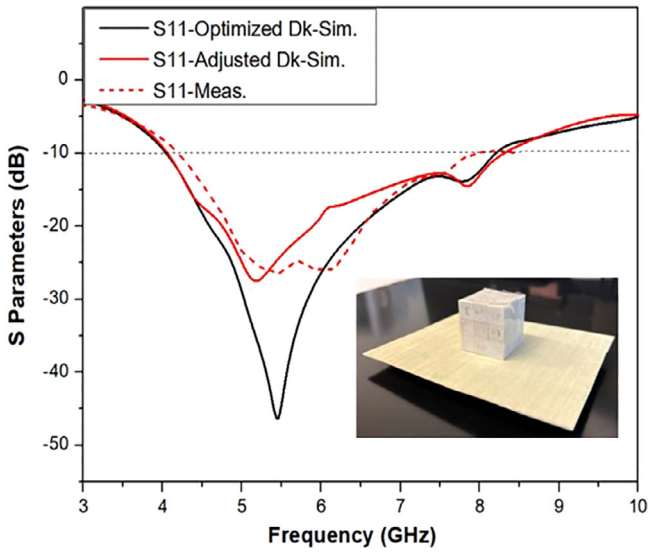

Fig. 4 *The simulated S parameters of the proposed dielectric resonator antenna (DRA) with optimized dielectric constants (black), and with the adjusted dielectric constants (solid red), and the measured S parameter with the adjusted dielectric constants (dashed red)*

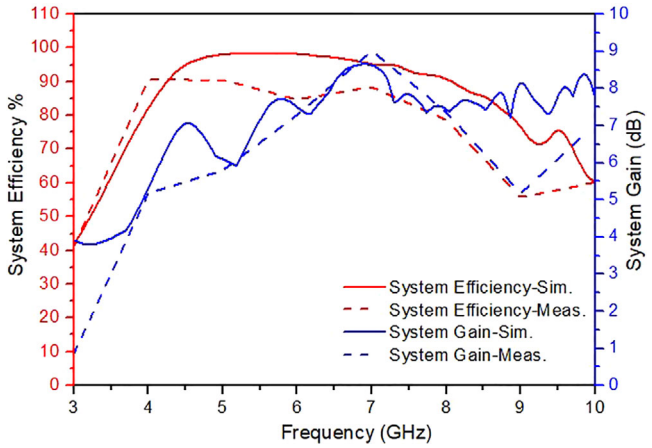

Fig. 5 *Comparison between the simulated (solid) and measured (dashed) system efficiency and gain*

for the other two modes in Figure 3. Because of the varying material distribution within our DRA, we can only approximately relate the current distribution to standard modes in a uniform rectangular DRA [22, 23].

Prototype and measurement: Materials with different dielectric constants listed in Table 1 are very difficult to realize with the exact same values. To facilitate prototyping of the proposed wideband DRA, Wavepro provided materials with adjusted dielectric constants, as indicated in Table 1 (values shown in parentheses). A total of 27 cubes are provided, each measuring 10 mm in size, composed of different materials as listed in Table 1 in parentheses. These cubes were then assembled into a single DRA. For the measurement setup, we fabricated a feed structure using Rogers RO4350B as the substrate and an SMA probe with a height of 7 mm. The prototyped DRA with the feed structure is shown in Figure 1c.

The performance of the DRA with adjusted dielectric constants was first verified in HFSS through full-wave simulation. Figure 4 shows the simulated *S* parameters for the optimized DRA with the exact dielectric constants (black), the adjusted dielectric constants DRA (solid red), and the measured *S* parameter of the implemented prototype (dash red). From Figure 4, it is clear that the bandwidth of the optimized DRA with adjusted dielectric constants is not affected by the small adjustment in dielectric constants of materials. The simulated and measured *S* parameters at the operating frequency were in relatively good agreement.

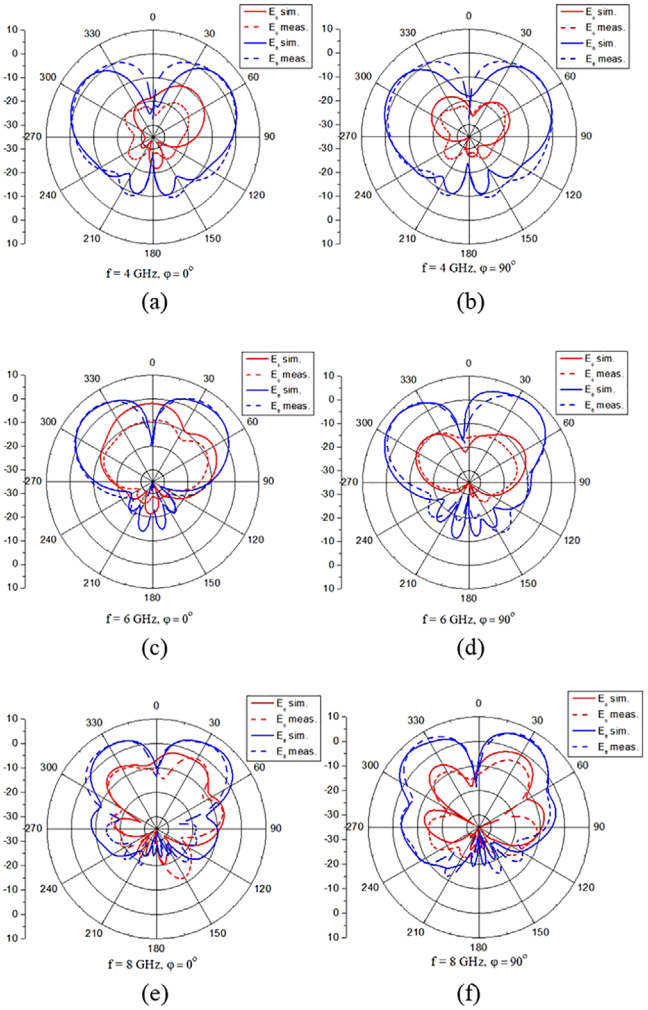

Fig. 6 *Radiation pattern at 4(a-b), 6(c-d), and 8(e-f) GHz. Solid lines are the simulation data, and dashed lines are the measured data. Red curves show E_Φ, and the blue curves are E_θ*

Table 2. Comparison of proposed work with the previous work

References	f_r (GHz)	FBW (%)	Size (λ_0^3)
[24]	3.5	30	0.64 (diameter) × 0.12 (height)
[25]	3.5	37	3.14 × 0.152 × 0.27
[26]	5	42.5	0.77 × 0.77 × 0.09
[27]	5	45.9	0.36 (diameter) × 0.18 (height)
[28]	8.4	58.2	0.64 × 0.28 × 0.268
[29]	6	60.2	1.5 (diameter) × 0.18 (height)
Our work	6	64.9	0.6 × 0.6 × 0.6

Next, the simulated and measured system efficiency and system gain versus frequency are plotted in Figure 5. The maximum simulated system efficiency achieved over the operating frequency range is 98%. The peak measured system efficiency is about 90.6%, reasonably close to the simulation. The peak measured system gain achieved is 9 dB at 7 GHz and matches well with the simulated data. To demonstrate the 3D radiation characteristics of the proposed wideband DRA, the radiation pattern of the antenna at 4, 6, and 8GHz is provided in Figure 6. A radiation null is observed at broadside, because the antenna is behaving similar to an electric monopole. The proposed DRA performance is compared with some prior arts [24–29] in Table 2 and is shown to display higher bandwidth with a relatively small footprint and volume. The DRA size in Table 2 is given in terms of free space wavelength at the centre frequency.

Conclusion: A compact wideband DRA with inhomogeneous material distribution was designed based on evolutionary optimization search within the specified and discretized volume. Then the optimized varying dielectric constants were rounded to the actual materials provided by the Wavepro to implement the optimized DRA design. The proposed design achieves a measured fractional bandwidth of 64.9% and a peak system efficiency of 90.6%, validating the design method.

Author contributions: **Trupti Bellundagi**: Data curation; formal analysis; investigation; methodology; software; validation; visualization and writing—original draft. **Binbin Yang**: Conceptualization; funding acquisition; investigation; methodology; project administration; resources; supervision and writing—review and editing.

Acknowledgements: This material is based upon work supported by the National Science Foundation under Grant No. 2138741.

Conflict of interest statement: The authors declare no conflicts of interest.

Funding information: National Science Foundation under Grant No. 2138741.

Data availability statement: The data that support the findings of this study are available from the corresponding author upon reasonable request.

Received: *10 September 2024* Accepted: *25 November 2024*
doi: 10.1049/ell2.70107

References

1 Long, S., McAllister, M., Shen, L.: The resonant cylindrical dielectric cavity antenna. *IEEE Trans. Antennas Propag.* **31**(3), 406–412 (1983)
2 Lai, Q., Almpanis, G., Fumeaux, C., Benedickter, H., Vahldieck, R.: Comparison of the radiation efficiency for the dielectric resonator antenna and the microstrip antenna at ka band. *IEEE Trans. Antennas Propag.* **56**(11), 3589–3592 (2008)
3 Kishk, A.A., Fong Lee, K., Kajfez, D.: Performance comparisons between dielectric resonator antennas and printed microstrip patch antennas at x-band. *Microwave J.* **49**, 90–104 (2006)
4 Guha, D., Kumar, C.: Microstrip patch versus dielectric resonator antenna bearing all commonly used feeds: An experimental study to choose the right element. *IEEE Antennas Propag. Mag.* **58**(1), 45–55 (2016)
5 Petosa, A., Ittipiboon, A.: Dielectric resonator antennas: A historical review and the current state of the art. *IEEE Antennas Propag. Mag.* **52**(5), 91–116 (2010)
6 Asadullah, Khan, M.U., Muhammad, A., Sharawi, M.S., Alathbah, M.: Singly-fed large frequency ratio composite dielectric resonator antenna for sub-6 ghz and mm-wave 5g applications. *IEEE Access* **12**, 67837–67846 (2024)
7 Chaudhuri, S., Mishra, M., Kshetrimayum, R.S., Sonkar, R.K., Chel, H., Singh, V.K.: Rectangular dra array for 24 ghz ism-band applications. *IEEE Antennas Wirel. Propag. Lett.* **19**(9), 1501–1505 (2020)
8 Attia, A., Hussein, A., Sharawi, M.S., Kishk, A.A.: Wideband circularly polarized millimeter-wave dra array for internet of things. *IEEE IoT J.* **10**(11), 9597–9606 (2023)
9 Chair, R., Kishk, A., Lee, K.F.: Wideband stair-shaped dielectric resonator antennas. *Microwaves, Antennas Propag, IET* **1**, 299–305 (2007)
10 Kishk, A.A.: Wide-band truncated tetrahedron dielectric resonator antenna excited by a coaxial probe. *IEEE Trans. Antennas Propag.* **51**(10), 2913–2917 (2003)
11 Bellundagi, T., Yang, B.: A novel shaped symmetric wideband dielectric resonator antenna by binary material optimization. In: 2024 United States National Committee of URSI National Radio Science Meeting (USNC-URSI NRSM), IEEE Boulder, CO, USA. pp. 68–69 (2024)

12 Alroughani, H., McNamara, D.A.: The shape synthesis of dielectric resonator antennas. *IEEE Trans. Antennas Propag.* **68**(8), 5766–5777 (2020)
13 Ozzaim, C., Ustuner, F., Tarim, N.: Stacked conical ring dielectric resonator antenna excited by a monopole for improved ultrawide bandwidth. *IEEE Trans. Antennas Propag.* **61**(3), 1435–1438 (2013)
14 Kishk, A.A., Zhang, X., Glisson, A.W., Kajfez, D.: Numerical analysis of stacked dielectric resonator antennas excited by a coaxial probe for wideband applications. *IEEE Trans. Antennas Propag.* **51**(8), 1996–2006 (2003)
15 Diaz, S., Diaz, M., Rajo-Iglesias, E., Pizarro, F.: 3-D-printed highgain multisection dra with symmetric radiation pattern. *IEEE Antennas Wirel. Propag. Lett.* **23**(5), 1458–1462 (2024)
16 Chaudhary, R.K., Srivastava, K.V., Biswas, A.: Variation of permittivity in radial direction in concentric half-split cylindrical dielectric resonator antenna for wideband application. *Int. J. RF Microw. ComputAided Eng.* **25**(4), 321–329 (2015)
17 Omar, M.F.M., Zubir, I.A., Kamal, S., Rajendran, J.A.L., Mohamed, J.J., Ahmad, Z.A., et al.: A critical review on the development of multigeometrical stacked wideband dielectric resonator antenna. *Alexandria Eng. J.* **100**, 111–141 (2024)
18 Yang, C., Xiao, Y., Leung, K.W.: A 3d-printing wideband multilayered inverted truncated conical dielectric resonator antenna with serrated ground. In: 2020 Cross Strait Radio Science Wireless Technology Conference (CSRSWTC), IEEE Fuzhou, China. pp. 1–3 (2020)
19 Xin, H., Liang, M.: 3-D-printed microwave and thz devices using polymer jetting techniques. *Proc. IEEE* **105**(4), 737–755 (2017)
20 Nayeri, P., Brennecka, G.: Wideband 3d-printed dielectric resonator antennas. In: 2018 IEEE International Symposium on Antennas and Propagation USNC/URSI National Radio Science Meeting, IEEE Boston, MA, USA. pp. 2081–2082 (2018)
21 Johnson, J.M., Rahmat-Samii, Y.: Genetic algorithm optimization and its application to antenna design. In: Proceedings of IEEE Antennas and Propagation Society International Symposium and URSI National Radio Science Meeting, IEEE Xiamen, China. vol. **1**, pp. 326–329 (1994)
22 Mongia, R.K.: Theoretical and experimental resonant frequencies of rectangular dielectric resonators. *IEE Proc H (Microwaves, Antennas Propag)* **139**(1), 98–104 (1992)
23 Yang, B., Kim, J., Adams, J.J.: Fundamental limits on substructure dielectric resonator antennas. *IEEE Open J. Antennas Propag.* **3**, 59–68 (2021)
24 Yang, T., Ren, J., Zhang, B., Liu, Y.T., Ma, T., Yin, Y.: Wideband diversity cylindrical dielectric resonator antenna based on multimode resonance. *IEEE Antennas Wirel. Propag. Lett.* **22**(9), 2205–2209 (2023)
25 Moayyed, F., Oskouei, H.D., Shirkolaei, M.M.: High gain and wideband multi-stack multilayer anisotropic dielectric antenna. *Progress In Electromagnet. Res. Lett.* **99**, 103–109 (2021)
26 Pan, Y.M., Zheng, S.Y.: A low-profile stacked dielectric resonator antenna with high-gain and wide bandwidth. *IEEE Antennas Wirel. Propag. Lett.* **15**, 68–71 (2016)
27 Chaudhary, R.K., Srivastava, K.V., Biswas, A.: A practical approach: design of wideband cylindrical dielectric resonator antenna with permittivity variation in axial direction and its fabrication using microwave laminates. *Microwave Opt. Technol. Lett.* **55**(10), 2282–2288 (2013)
28 Chaudhary, R.K., Baskey, H.B., Srivastava, K.V., Biswas, A.: Synthesis and microwave characterization of $(Zr_{0.8}\ Sn_{0.2})\ TiO_4$–epoxy composite and its application in wideband stacked rectangular dielectric resonator antenna. *IET Microwaves, Antennas Propag* **6**(7), 740–746 (2012)
29 Xia, Z.-X., Leung, K.W., Lu, K.: A 3D-printed wideband multi-ring dielectric resonator antenna. *IEEE Antennas Wirel. Propag. Lett.* **18**(10), 2110–2114 (2019)